Downwelling along the Northeastern Coasts of the Eastern Mediterranean

YIZHAK FELIKS*

Israel Institute for Biological Research, Department of Mathematics, Ness-Ziona, Israel

(Manuscript received 13 December 1989, in final form 11 October 1990)

ABSTRACT

The most prominent winter storms in the eastern part of the Eastern Mediterranean are known as Cyprus cyclones. The surface wind speed is between 15–30 m s^{-1}, and about five such cyclones occur in a typical winter. The cyclone radius is between 500 and 1500 km. The evolution of the sea structure under such atmospheric forcing is examined with a two-dimensional numerical model in the vertical cross section perpendicular to the shore line. Two distinct regions result in the sea. A downwelling zone near the coast, about 100 km wide, and a horizontally homogeneous zone in the open sea, where vertical mixing is the important dynamical process. In the open sea the final profiles turn out to be similar to those observed in the Levantine Intermediate Water (LIW) in their formation region. We suggest that the LIW forms in the region under the influence of these Cyprus cyclones.

In the downwelling zone the 14°–17°C isotherms decline by more than 250 m. This water has the same T–S properties as the water in the anticyclonic eddies found along the Asia Minor coast and other parts of the Eastern Mediterranean. A very deep mixed layer is obtained, deeper than 300 m. The water in the downwelling zone near the sea surface is warmer by 0.5°–1°C than in the open sea. This last result is observed in winter IR satellite images.

The downwelling rate increases with increasing wind stress and decreasing horizontal eddy coefficient. This rate is not influenced by the evolution in the mixing layer.

Along the coast in the downwelling front a prominent jet developed. The scale of the jet is proportional to the square root of the horizontal eddy coefficient.

1. Introduction

The LIW forms during the winter season mainly in February along the Asia Minor Coast (between 27° and 36°E). At this time an overturning of the water column occurs down to 100–200 m due to cooling of the water in the upper layers to about 16°C by the winter storms. The water column therefore becomes homogeneous in the upper 100–200 m (Wust 1961).

Warm and salty core eddies have been shown to exist in the Eastern Mediterranean (EM) (Feliks and Itzikowitz 1987; Hecht et al. 1988; Ozsoy et al. 1989). In those eddies the 14°–16°C isotherms decline by 100–300 m over a horizontal distance of about 50 km. The same decline was observed in the 38.75–39.05 isohalines. The water type in the core of the eddy, down to 450 m is that of the Levantine Intermediate Water (LIW) in its formation region along the Asia Minor Coast. In some eddies their signal was observed down to depths of 800–900 m, and they could persist in the region for more than a year. Feliks and Itzikowitz analyzed historical data and found that such eddies were observed along the coast of Asia Minor and around latitude 34°N. Their conclusion was that the source of these eddies is probably along the coasts of Asia Minor where the LIW is assumed to form. Ozturgut (1976) found sharp fronts, jets and eddies along the Asia Minor Coast and Antalya Basin. Ozsoy et al. (1989) found in that region a series of anticyclonic eddies; some are deep and exist for a long time. The LIW are found in the core of the eddies.

Along the Asia Minor Coast a permanent westerly current seems to exist. This current can be masked by anticyclonic eddies (Ozsoy et al. 1989). Some measurements on the shelf of the Asia Minor current show that its mean speed is about 10 cm s^{-1} (Unluta et al. 1983).

The formation of the warm and salty water, found in the core of the anticyclonic eddies along Asia Minor, can not be explained by a simple overturning process since the 15.5°C isotherm is observed at a depth of about 450 m warmer water (17°C) is observed at a depth of 200 m, and the eddy signal is observed at depths of 800–900 m.

In the following, using a numerical model in the sea, we show that under the atmospheric forcing of five successive winter storms, the LIW can form, and that near the coasts of Asia Minor and the northeast coast of the Mediterranean intensive downwelling develops

* Present affiliation: Dept. of Atmospheric Sciences, University of California, Los Angeles.

Corresponding author address: Dr. Yizhak Feliks, Dept. of Atmospheric Sciences, UCLA, Los Angeles, CA 90024-1565.

which brings the LIW down to 450 m. A longshore geostrophic current develops resembling the Asia Minor current. In section 2 we describe the characteristics of Cyprus cyclones. In section 3 we describe the model equations and the numerical technique used to solve them. In section 4 the results of the numerical model are discussed.

2. Cyprus cyclones

During winter the most prominent storms in the eastern part of the EM are due to cyclones centered around Cyprus (Fig. 1). The radius of the cyclones is between 500 and 1500 km. The surface winds speed is between 15 and 30 m s^{-1}. The air temperature near the sea surface is about 10°C. The Cyprus cyclones normally stall in the region for 2–4 days and then move northeastward. Due to lack of observations over the sea, the description of Cyprus cyclone is far from complete. During a typical winter about five such cyclones are observed, and in some years even ten are observed. However, in warm winters the cyclones are rare and even absent (Barkan, private communication; Alpert et al. 1989). Between successive cyclones there is a period of several days of calm weather.

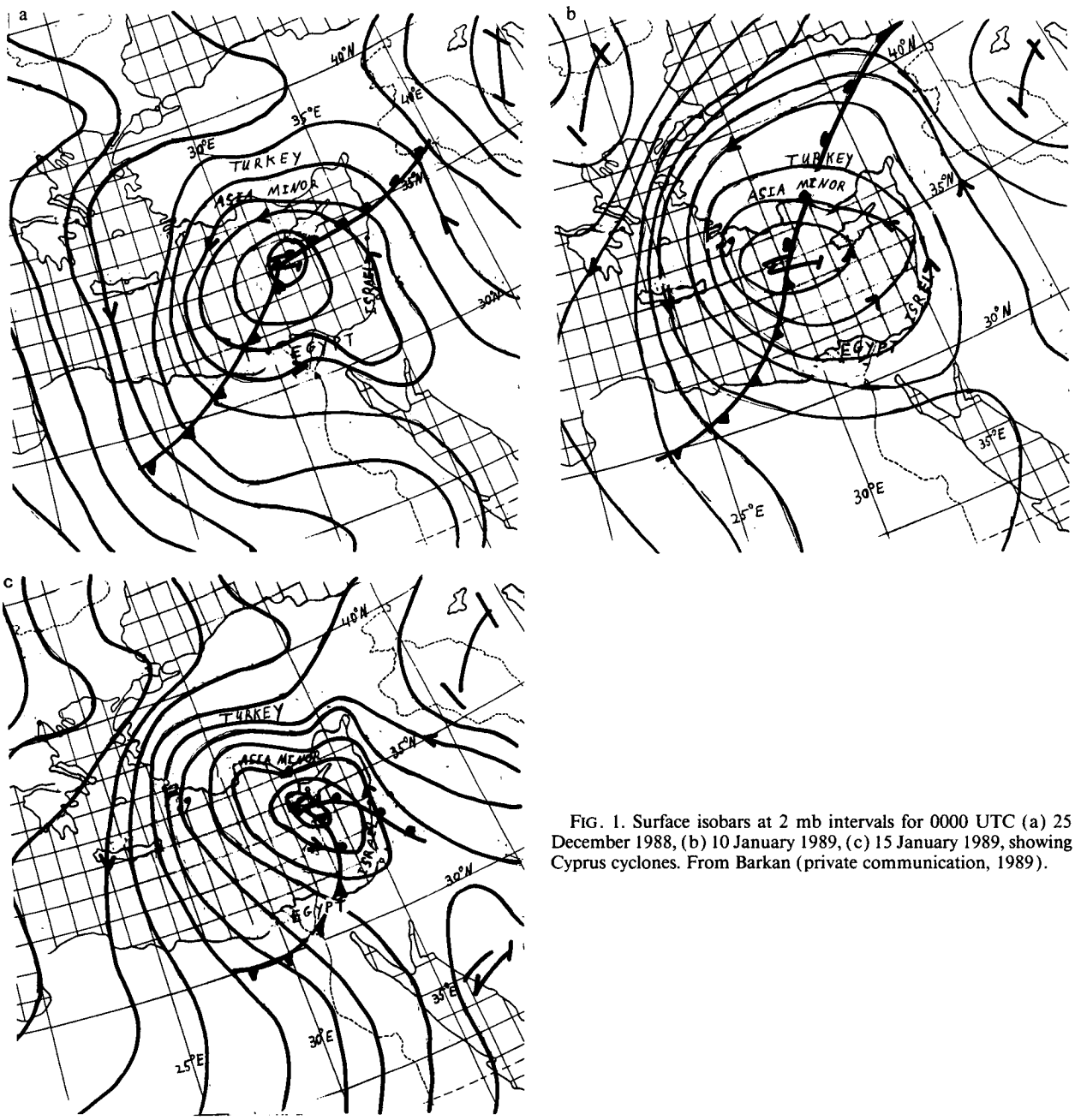

FIG. 1. Surface isobars at 2 mb intervals for 0000 UTC (a) 25 December 1988, (b) 10 January 1989, (c) 15 January 1989, showing Cyprus cyclones. From Barkan (private communication, 1989).

Figure 1 shows the synoptic surface maps during three Cyprus cyclones, 25 December 1988 and 10 and 15 January 1989. Easterly winds blow along the Asia Minor coast and southerly winds along the northern part of the Eastern Mediterranean coast. The measured wind speed in the 10 January cyclone reached 25 m s^{-1}, and persisted about 2 days. Such winds favor coastal downwelling.

3. The model

a. Basic equations

The Boussinesq incompressible approximation of the equations of motion in a vertical cross section perpendicular to the coast (x, z) are

$$\frac{\partial u}{\partial t} = fv - \frac{1}{\rho}\frac{\partial p}{\partial x} - u\frac{\partial u}{\partial x} - w\frac{\partial u}{\partial z} + \frac{\partial}{\partial z}\left(K_m\frac{\partial u}{\partial z}\right) + K_h\frac{\partial^2 u}{\partial x^2} \quad (3.1)$$

and

$$\frac{\partial v}{\partial t} = -fu - u\frac{\partial v}{\partial x} - w\frac{\partial v}{\partial z} + \frac{\partial}{\partial z}\left(K_m\frac{\partial v}{\partial z}\right) + K_h\frac{\partial^2 v}{\partial x^2}. \quad (3.2)$$

The third equation of motion is replaced by the hydrostatic approximation

$$\frac{\partial p}{\partial z} = -\rho g. \quad (3.3)$$

The incompressible continuity equation is

$$\frac{\partial u}{\partial x} + \frac{\partial w}{\partial z} = 0. \quad (3.4)$$

The thermodynamic energy evaluation is

$$\frac{\partial T}{\partial t} = -u\frac{\partial T}{\partial x} - w\frac{\partial T}{\partial z} + \frac{\partial}{\partial z}\left(K_e\frac{\partial T}{\partial z}\right) + A_h\frac{\partial^2 T}{\partial x^2}. \quad (3.5)$$

The salinity conservation equation is

$$\frac{\partial S}{\partial t} = -u\frac{\partial S}{\partial x} - w\frac{\partial S}{\partial z} + \frac{\partial}{\partial z}\left(K_s\frac{\partial S}{\partial z}\right) + B_h\frac{\partial^2 S}{\partial x^2}. \quad (3.6)$$

The height of the sea surface equation is

$$\frac{\partial h}{\partial t} = -u\frac{\partial h}{\partial x} + w. \quad (3.7)$$

The equation of state is

$$\rho = 1 + 10^{-3}\sigma_t(S, T, p), \quad (3.8)$$

where $\sigma_t(S, T, p)$ is computed as in Fofonoff and Millard (1983).

Substituting (3.8) into (3.3) and integrating from the sea surface to a depth z, we have

$$p(z) = p(s) + g(h - z) + 10^{-3}g\int_z^h \sigma_t dz \quad (3.9)$$

where $p(s)$ is the pressure at the sea surface; K_h, A_h, B_h are the horizontal eddy diffusivities of momentum, temperature, and salinity and K_m, K_e and K_s the corresponding vertical components.

Following Madala and Piacsek (1977) we average equations (3.1), (3.2) with respect to depth $H(x)$ of the sea bottom

$$(\bar{\ }) = \frac{1}{H}\int_{-H}^{0}(\ )dz,$$

and assuming that the sea surface deviation, h, is two orders of magnitude smaller than the ocean depth, we have

$$\frac{\partial \bar{u}}{\partial t} = f\bar{v} - g\frac{\partial h}{\partial x} + \bar{A} \quad (3.10)$$

$$\frac{\partial \bar{v}}{\partial t} = -f\bar{u} + \bar{B} \quad (3.11)$$

and

$$\frac{\partial h}{\partial t} = -\frac{\partial (H\bar{u})}{\partial x} - u\frac{\partial h}{\partial x}, \quad (3.12)$$

where

$$A = -g10^{-3}\frac{\partial}{\partial x}\int_Z^h \sigma_T dz - u\frac{\partial u}{\partial x} + \frac{\partial}{\partial z}K_m\frac{\partial u}{\partial z} + K_h\frac{\partial^2 u}{\partial x^2} - w\frac{\partial u}{\partial z},$$

$$B = -u\frac{\partial v}{\partial x} + \frac{\partial}{\partial z}K_m\frac{\partial v}{\partial z} + K_h\frac{\partial^2 v}{\partial x^2} - w\frac{\partial v}{\partial z},$$

$$\bar{A} = -\frac{g}{H}10^{-3}\int_{-H}^{0}\int_z^h \frac{\partial \sigma_T}{\partial x}\,dl\,dz - \frac{1}{H}\int_{-H}^{0} u\frac{\partial u}{\partial x}dz + \frac{\tau_s^x}{H} - \frac{\tau_b^x}{H} + \frac{K_h}{H}\frac{\partial^2 (H\bar{u})}{\partial x^2} \quad (3.13)$$

and

$$\bar{B} = -\frac{1}{H}\int_{-H}^{0} u\frac{\partial v}{\partial x}dz + \frac{\tau_s^y}{H} - \frac{\tau_b^y}{H} + \frac{K_h}{H}\frac{\partial^2 (H\bar{v})}{\partial x^2},$$

$\vec{\tau}_s$ is the wind stress at the sea surface and $\vec{\tau}_b$ is the bottom stress.

Subtracting (3.10) from (3.1) and (3.11) from (3.2) we have

$$\frac{\partial u'}{\partial t} = fv' + A - \bar{A} \quad (3.14)$$

and

$$\frac{\partial v'}{\partial t} = -fu' + B - \bar{B},$$

where $u = \bar{u} + u'$, $v = \bar{v} + v'$.

Equations (3.14) are independent on terms governing external gravity waves. Together with Eqs. (3.5), (3.6) they govern the slow moving baroclinic mode (mostly internal waves) and can be solved in large time intervals. Equations (3.10)–(3.12) govern the fast moving external gravity modes and need to be solved for small time intervals.

In the numerical simulation $K_h = 10^7$ cm^2 s^{-1}, $A_h = B_h = 5 \times 10^6$ cm^2 s^{-1}.

b. The vertical exchange coefficients

The closure of the model requires an explicit formulation of the exchange coefficients in terms of the dependent variables. The formulation adopted follows Pandolfo and Jacobs (1973), with some modification by Huss and Feliks (1981). We assume three stability regimes, which are identified by the local Richardson number, i.e.

$$\mathrm{Ri} = N^2 \Big/ \left(\frac{\partial \mathbf{V}_h}{dz}\right)^2 \tag{3.15}$$

where N is the Brunt–Väisälä frequency, and $\mathbf{V}_h = (u, v)$.

For convenience of notation we adopt the concept of mixing length, without insisting on its physical content

$$l = k(\tilde{z} + z_0) \Big/ \left[1 + 4\left(\frac{\tilde{z} + z_0}{z_m}\right)^{5/4}\right] \tag{3.16}$$

where

$$\tilde{z} = z\left(\frac{z}{-H} - 1\right)$$

and $z_0 = 1$ cm; $k = 0.4$ is von Kármán's constant. $z_m = 35$ m is the depth where the maximal value of 1 is attained.

The exchange coefficients in the three regimes are defined:

$0 < \mathrm{Ri}$:

$$K_m = l^2\left(1 + \frac{\mathrm{Ri}}{3}\right)^{-1/2}\left|\frac{\partial \mathbf{v}_h}{\partial z}\right| \tag{3.17}$$

$$K_e = l^2(1 + \mathrm{Ri})^{-3/2}\left|\frac{\partial \mathbf{v}_h}{\partial z}\right|$$

$\mathrm{Ri}_c < \mathrm{Ri} < 0$:

$$K_m = l^2(1 - \alpha \mathrm{Ri})^{-2}\left|\frac{\partial \mathbf{v}_h}{\partial z}\right| \tag{3.18}$$

$$K_e = K_m(1 - \alpha \mathrm{Ri})^{-1}$$

$\mathrm{Ri} < \mathrm{Ri}_c$:

$$K_e = l^2 h_p |N| / k^2 \tag{3.19}$$

$$K_m = A_w |\mathrm{Ri}|^{-1/6} K_e;$$

$h_p = 0.9$ is Priestly's heat convection constant, $\alpha = -0.3$, $\mathrm{Ri}_c = -0.03$, $A_w = (k^2/h_p)^{1/2} = 0.56$.

c. Boundary conditions

The horizontal components of the current u, v are assumed to vanish at the land water boundary. At the ocean–air interface u and v are obtained by the assumption of continuity of momentum flux through the sea–air interface, i.e.

$$\rho K_m \frac{\partial u}{\partial z} = \tau_s^x, \quad \rho K_m \frac{\partial v}{\partial z} = \tau_s^y. \tag{3.20}$$

At the lower boundary $z = -H(x)$, u and v are assumed to vanish, i.e.

$$u' = -\bar{u}, \quad v' = -\bar{v}, \tag{3.21}$$

and the vertical velocity, w, is assumed to vanish. At the open lateral boundary

$$\frac{\partial \bar{u}}{\partial x} = \frac{\partial \bar{v}}{\partial x} = \frac{\partial u}{\partial x} = \frac{\partial v}{\partial x} = \frac{\partial p}{\partial x} = \frac{\partial T}{\partial x} = \frac{\partial S}{\partial x} = 0; \tag{3.22}$$

h at the lateral boundaries is computed according to (3.10), i.e.

$$\frac{\partial h}{\partial x} = \frac{f\bar{v} + \bar{A} - \partial \bar{u}/\partial t}{g}. \tag{3.23}$$

The heat budget at the sea surface is due to 1) sensible heat flux to the atmosphere, H_s, 2) the evaporation heat loss, H_l, and 3) heat flux from the sea toward the sea surface, H_w. In our simulation the radiation of energy by the ocean surface is neglected. We use the bulk formulae from Thompson (1974) to evaluate each term.

$$H_s = C_d \rho_a C_p (T - T_a) U \tag{3.24}$$

where $C_d = 1.3 \times 10^{-3}$ is the drag coefficient, $\rho_a = 1.24\ 10^{-3}$ g cm^{-3} the air density, $C_p = 0.24$ cal (g °C)$^{-1}$ the heat capacity of air, T_a is the atmospheric temperature, U wind speed.

$$H_l = C_d L \rho_a (q_w - q_a) U \tag{3.25}$$

where $L = 584$ cal g^{-1} is the heat evaporation and $q_a = 0.622 \times \mathrm{RH} * P_s(T_a)/760$, RH is the relative humidity of air, and $P_s = 5.064 \exp(0.062T)$ the atmospheric vapor pressure of water. Also, $q_w = q_a(T)$ when RH = 1.

$$H_w = c_{pa} \rho_0 K_e \frac{\partial T}{\partial z} \tag{3.26}$$

$c_{pa} = 1$ cal (g °C)$^{-1}$ is heat capacity of water.

The salinity flux at the sea surface was assumed to vanish.

d. Numerical aspects

The equations are applied to a grid contained within a vertical plane extending in the x-coordinate perpendicular to the assumed coast line. A staggered grid is used in the horizontal coordinate as in Fig. 2. The horizontal grid interval was taken as $\Delta x = 5$ km and 92 grid points, including boundaries, are assumed at each level. 23 information levels are taken in the sea, at the depths of: 0.9, 5.6, 11.2, 16.7, 22.3, 27.9, 33.5, 39.1, 44.7, 67.0, 89.4, 111.7, 134.1, 178.8, 290.5, 514.0, 849.2, 1296.1, 1631.3, 1854.7, 1966.5, 1988.8, 2000 m.

A forward time scheme is used to approximate the time derivative. The "component-by-component splitting method" is used to solve the prognostic equations (Marchuk 1975). Horizontal advective terms are approximated by the Lax–Wendroff scheme, and the horizontal diffusion is solved explicitly. Vertical diffusion and advection are solved implicitly to allow large time steps. u, v, w, T and S are computed on the information levels, K_e, K_m, Ri and N are computed at the midlevels.

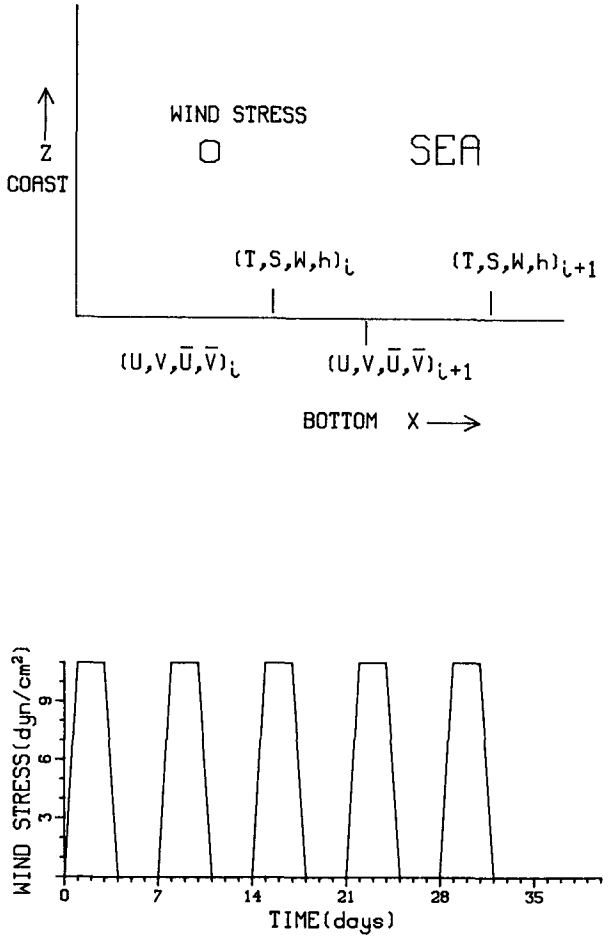

FIG. 2. (a) Arrangement of variables on the staggered-grid schematic diagram of the model domain. (b) The forcing function—the wind stress.

The time interval in Eqs. (3.5), (3.6) and (3.14) is $\Delta t = 900$ s, and in (3.10)–(3.12) it is 15 s. This smaller time interval is due to external gravity waves appearing in the equations. The stability condition for our case, i.e., staggered grid in the horizontal coordinate, is given in Haltiner and Williams (1980, p. 142). The truncation error of the numerical scheme is $\Delta t + \Delta x^2 + \Delta z^2$.

4. The numerical results

In the following simulation the atmospheric forcing consists of five cyclones. The cyclone duration is taken as 4 days each. Every cyclone has only a longshore component. The wind stress increases linearly in the first day from zero to 11 dyn cm^{-2} (18 m s^{-1}), this speed is held constant for 2 days and then decreases linearly to zero during day 4 (Fig. 2). The air temperature is taken to be 10°C. In between storms we assume a period of 3 days of calm weather, i.e., a weak wind of 3 m s^{-1} in the cross-shore direction, and air temperature of 16°C. The above atmospheric assumptions roughly characterize the weather in the eastern Levantine Basin during winter.

Heat flux from the sea to the atmosphere occurs mainly during the cyclone period because the flux is proportional to wind speed (3.24), (3.25). During the calm between the two storms, the wind speed is smaller by an order of magnitude than during the storm, while the air temperature is usually higher in the calm period. So the heat flux in the calm period is smaller by at least one order of magnitude. The short calm period of 3 days between the cyclones is shorter than the week or two typically observed. However, about 3 days after the storm ends, the temperature and salinity fields almost do not change; for saving computation time we applied the next storm only 3 days after the end of the previous storm. After the fifth cyclone we continue the simulation for 8 additional days of calm weather. The temperature and salinity fields remain almost the same after day 3.

The initial profiles of temperature, salinity and Brunt–Väisälä frequency are shown in Fig. 3. The profiles were measured 100 km south of Turkey in October 1983, i.e., at the end of the autumn, when the salinity reaches its maximum value near the sea surface (39.5). In the upper 50 m we still observe a sharp thermocline. The high salinity water formed during the previous summer due to intensive evaporation. The minimum at 50 m is due to the North Atlantic water, which penetrates from the Strait of Gibraltar all the way to the eastern boundary of the Mediterranean Sea (Wust 1961). At the depth of 100 m we find the LIW as shown by the local salinity maximum of 39. The Rossby radius of deformation is 11.7 km. We assumed that u, v, w and $\partial p/\partial x$, $\partial T/\partial x$, $\partial S/\partial x$ vanish initially.

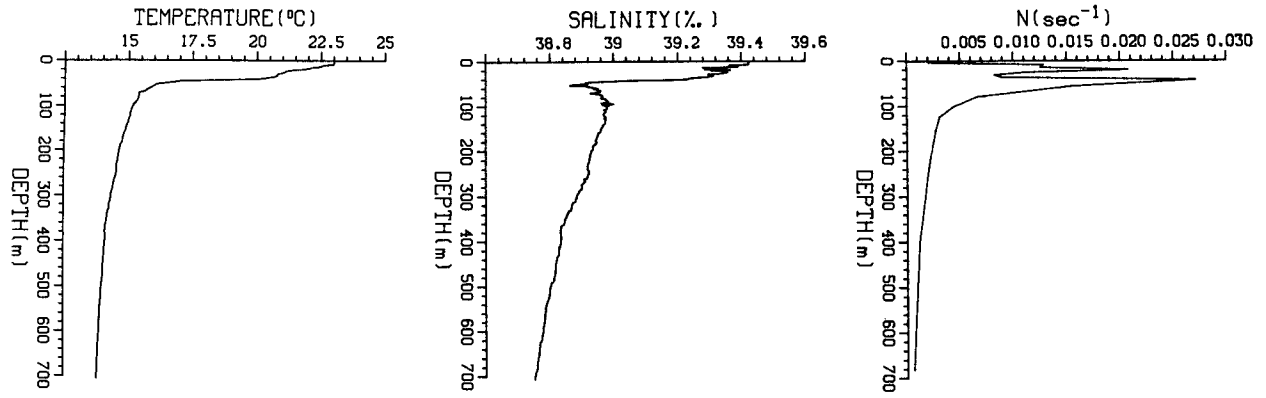

FIG. 3. The initial profiles of (a) temperature, (b) salinity, (c) Brunt-Väisälä frequency. Profiles were measured 100 km south of Turkey in October 1983.

a. The open sea

In Figs. 4 and 5 the temperature and salinity fields are shown before each storm and at the end of the integration. In Fig. 6 the vertical profiles of temperature and vertical exchange coefficient are shown in each storm. The results show two distinct regions: the coastal region, where the isotherms have a significant distortion about 100 km width, and the open sea region, where the temperature and salinity fields have no horizontal

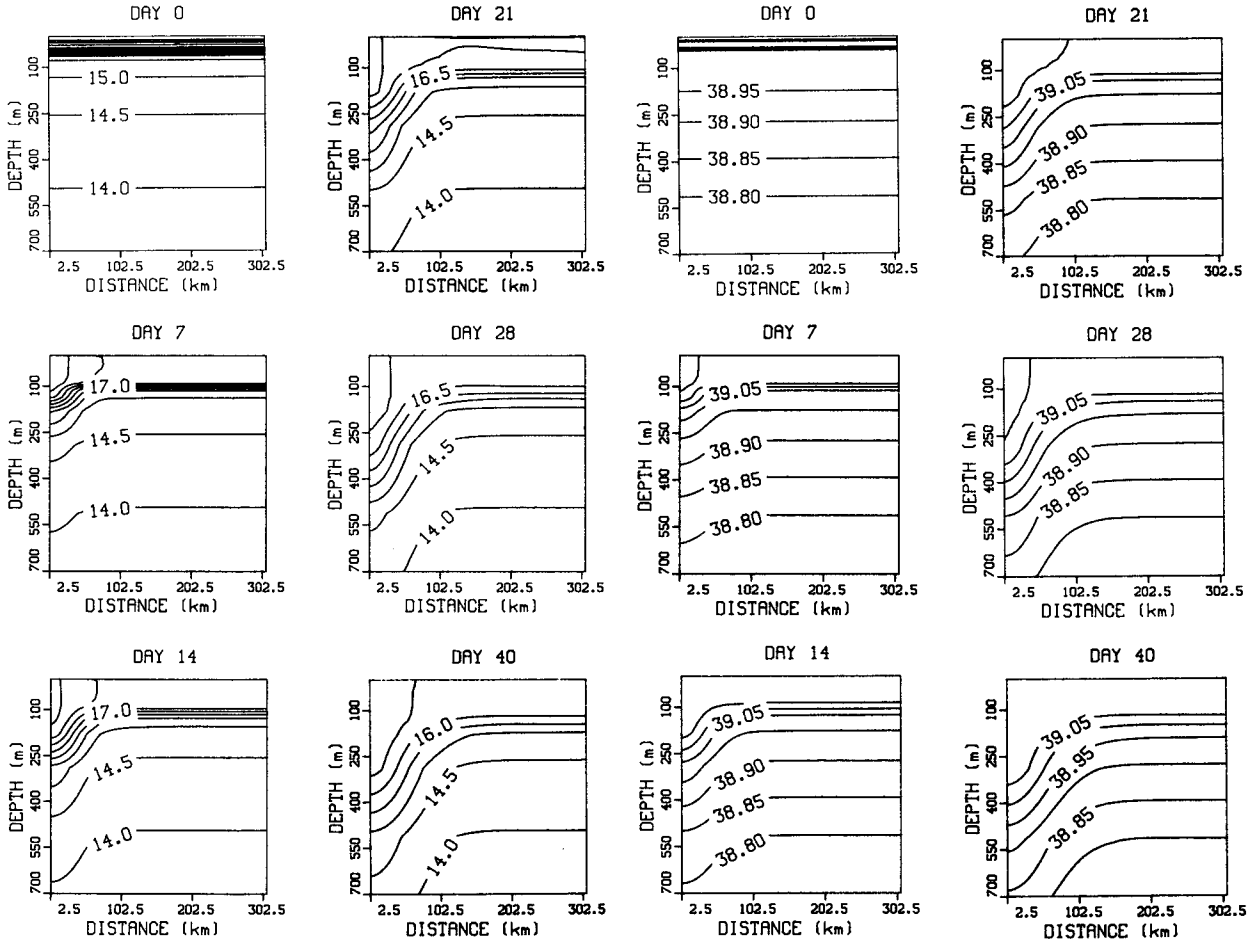

FIG. 4. Temperature field before each storm and at the end of the integration. Values in °C.

FIG. 5. Salinity field before each storm and at the end of the integration. Values in parts per thousand.

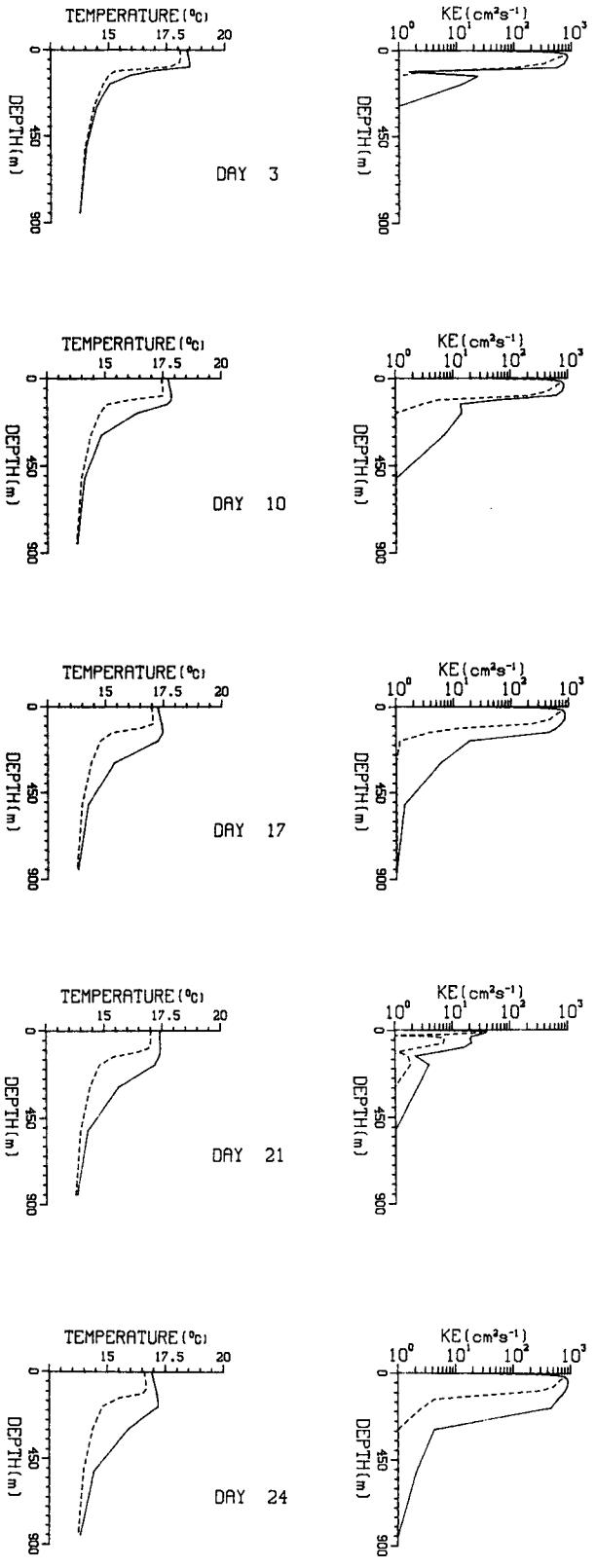

FIG. 6. Vertical profiles of temperature and vertical exchange coefficient for heat, K_e, 20 km off the coast in the downwelling zone (——), and 350 km off coast in the open sea (-----).

variation. Because the dynamics in this region is simple, we first analyze the numerical results from the open sea.

In the first storm the strong seasonal thermocline is eroded in the upper 70 m, and an almost isothermal and isohaline distribution is observed in this layer. In each successive storm the mixed layer penetrates to deeper layers. During the interval of calm weather, the mixed layer depth does not change. In each storm the water in the mixed layer cools due to heat flux from the sea to the atmosphere and entrainment of cold water from below, while the water below the mixed layer in the entrainment zone becomes somewhat warmer due to mixing with warm water from above. In the salinity field the process is similar. Deepening of the mixed layer brings about a decrease in salinity, mainly due to mixing with the North Atlantic inflow water and to a lesser extent with the water deeper below, (LIW), which is less saline than the surface water. So, at the end of the integration a homogeneous column of about 150 m is observed. The intensive vertical mixing is mainly due to the strong winds blowing during the cyclone period. The overturning conditions, which develop in the upper layer of the sea, enhance the mixing rate.

The impact of storms decrease with their sequential history (the most important is the first one, the second most important is the second one, etc.).

At the end of the integration, temperature in the upper 150 m is about 16°C, and the salinity is about 39.05. This water type has the same T–S properties as the LIW in its formation region (Wust 1961).

Examining the different terms in the thermodynamic equation (3.5) for the open sea (350 km off coast) shows that only the vertical diffusion is important in the evolution of the temperature and salinity profiles. The other terms are much smaller as can be anticipated from the horizontal homogeneity of the fields and, the smallness of the vertical velocity and the temperature below the mixing layer almost does not change during the integration period (Fig. 6). During mixing the upper layer cooled while the lower layer became warmer. As time goes on these two layers expand and penetrate downward. A short time after the cyclone ends, the vertical mixing stops and the vertical exchange coefficient decreases by an order of magnitude as shown in Fig. 6 for day 17 and day 21. We note that in the real case, where eddies are found, the horizontal and vertical advection can be important in the evolution.

b. The downwelling zone

In the coastal region we observe an intensive downwelling at all levels (Figs. 4, 5 and 6). During each cyclone the isotherms and isohalines sink by about 50–70 m, thus after five cyclones they sink by more than 250 m. The downwelling is observed also at depths of 800 m and more. The downwelling zone begins near

the coast and later expands toward the open sea, reaching a width of more than 100 km by the end of the integration. Two days after the storm ends, the downwelling stops (Fig. 7).

Weak inertial oscillations in the temperature and salinity fields are observed everywhere (Fig. 7). The temperature increases during the cyclone period, while in the calm period the rate of increase slows. So three days after the cyclone ended the rate is 0.01°C day^{-1}.

In the downwelling zone a very deep mixed layer (more than 300 m) is created. Penetration of the mixing downward in the downwelling zone is shown in Fig. 6 by the increase of K_e with depth as time goes on. During the cyclone an inversion develops in the upper layers of the downwelling zone. This inversion is caused mainly by horizontal advection of cold water from the open sea toward the coast. Cooling of the upper layers by heat flux to the atmosphere is much smaller. In the open sea, on the other hand, where advection is negligible, no significant inversion develops. The inversion disappears some days after the storm ends. This comes about because the mean (over inertial period) horizontal advection becomes very small as the cyclone ends (see below), while an intense vertical mixing still persists due to the instability of water in the inversion. The persistent inversion is the result of formulation of the mixing. In the model there is no convective adjustment except Richardson number-dependent vertical diffusion.

The warm band in the downwelling zone reaches the sea surface (Fig. 4). Can it be detected from IR images of the sea surface temperature? In Fig. 8 two images from winter of 1987 and 1988 are shown. Along the coasts of Asia Minor and the north east coast of the EM, indeed, a strip of warm water is truly observed. The water in the strip is warmer by 1°C than the water in the open sea. The width of the strip is about 50 km. Our interpretation is that this warm strip is the surface manifestation of the downwelling zone.

The last temperature and salinity profiles obtained in our simulation in the downwelling zone (Figs. 4 and 5 for day 40) bear a close similarity to the profiles observed in the anticyclonic eddies of the EM by Feliks and Itzikowitz (1987), Brenner (1989), Ozsoy et al. (1989). Such an eddy is shown in Fig. 9. This eddy is found in October its center is located at 34°N, 34°E. We suggest that this eddy was formed in the previous winter as discussed by Feliks and Itzikowitz.

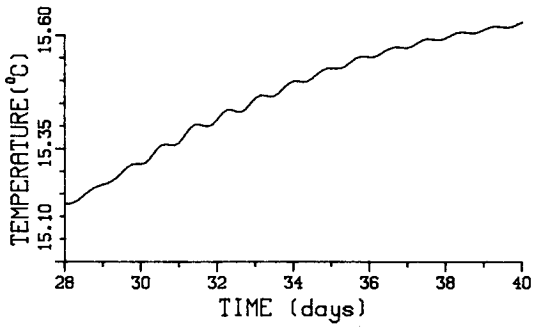

FIG. 7. Time series of the temperature between days 28 and 40 (the storm is between days 28 and 31) 55 km offshore at depth of 290.5 m.

c. *The currents*

First, we analyze the average (with respect to depth) current ($\bar{u}$, $\bar{v}$). The cross-shore component, $\bar{u}$, is very small. Near the coast it is about 0.001 cm s^{-1} and in the open sea it is about 0.03 cm s^{-1}. We note that our domain is 450 km long, while the external Rossby radius of deformation is 1750 km so we except that the cross-shore flow will be small (Csanady 1984, pp. 44 and 90). Inertial oscillations are observed in that component during the cyclones as well as calm periods.

During a cyclone, $\bar{u}$ is always directed toward the coast causing piling up of the sea surface, while during the calm period it changes its direction at times. The longshore component, $\bar{v}$, is almost in geostrophic balance. From the equation for the cross-shore velocity (3.10) the model shows that the longshore component is almost in geostrophic balance with the pressure gradient, as the other terms are smaller by more than two orders of magnitude. We note that the pressure in this case has two parts: one is due to the height of the sea surface and the other is due to the average (with respect to depth) pressure caused by density.

From the equation for the longshore component of the velocity (3.11), the model shows that changes in $\bar{v}$ are mainly due to changes in the wind stress and bottom stress. During the storms the surface stress exceeds the bottom stress and so the speed of $\bar{v}$ increases. As the storm ends the bottom stress becomes dominant, and the speed of $\bar{v}$ decreases (Fig. 10). Examination of the bottom stress $K_m(\partial v/\partial z)$ (Fig. 11) shows that its integral over a full (storm and calm) period is smaller than the wind stress acting on the sea surface during the same period, i.e. the momentum transferred to the sea by the wind stress during the storm is larger than the momentum removed from the sea by the bottom stress during the storm and calm period. However, as the speed of $\bar{v}$ increases more momentum is removed from the sea by bottom stress, and the growth rate of $\bar{v}$ slows.

In the upper 300 m and in the 10 m adjacent to the bottom, u and v differ significantly from $\bar{u}$ and $\bar{v}$. In Fig. 12 the longshore and cross-shore components are shown as functions of time 55 km offshore at a depth of 11.7 m. Inertial oscillations are observed in both components. The oscillation amplitude decays with depth, so at depth of 300 m it is smaller by more than one order of magnitude. During the calm interval this oscillation decays, while during the cyclone the amplitude of the oscillation increases. The inertial oscil-

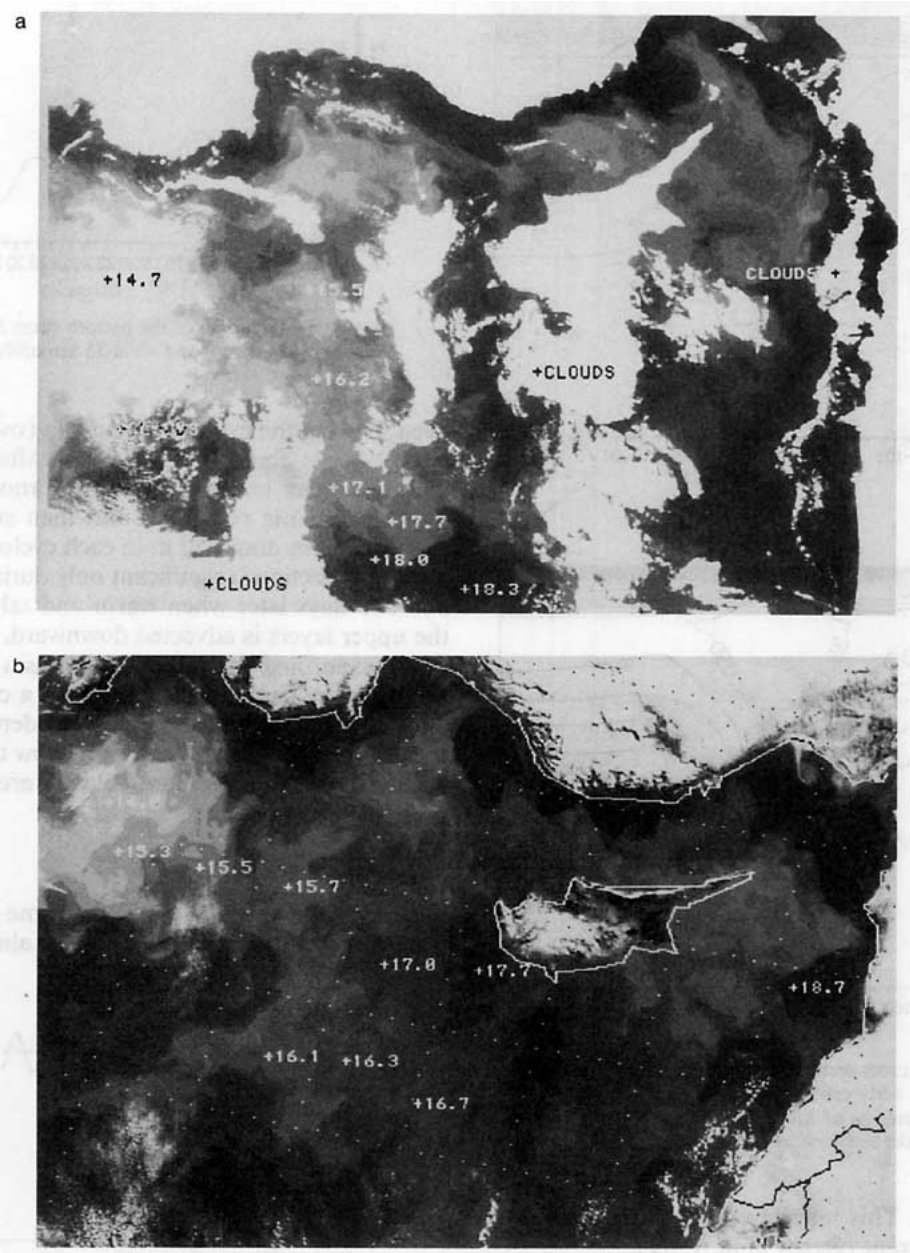

FIG. 8. Infrared image of the sea surface showing spatial structure of surface temperature of the eastern Levantine Basin on (a) 31 December 1987 and (b) 7 January 1988. The dark areas are warm water and the gray-white, cold water.

lations penetrate to a gradually increasing depth by momentum diffusion. For a detailed discussion see Gonella (1971). In the calm interval the mean (over inertial period) of u is very small, while during the storm the mean is about 30 cm s^{-1} and is directed toward the coast. So, the mean advection is important only during the cyclones when cold water from the open sea is advected toward the coast. As noted above, this advection caused the development of the inversion in the upper layers. In Fig. 13 the vertical cross section of u and v is shown three days after the fourth cyclone ended. In the longshore component in the downwelling zone, a jet of 100 km width and 300 m deep is observed. Its maximum is attained about 50 km off shore, near the sea surface. This jet is the result of geostrophic adjustment to the pressure field. We continue to run the model without any external forcing until day 115. The jet strength decreases with time. Its maximum speed after 55 days was 20 cm s^{-1}, after 75 days 15 cm s^{-1}, after 95 days 10 cm s^{-1} and after 115 days it became

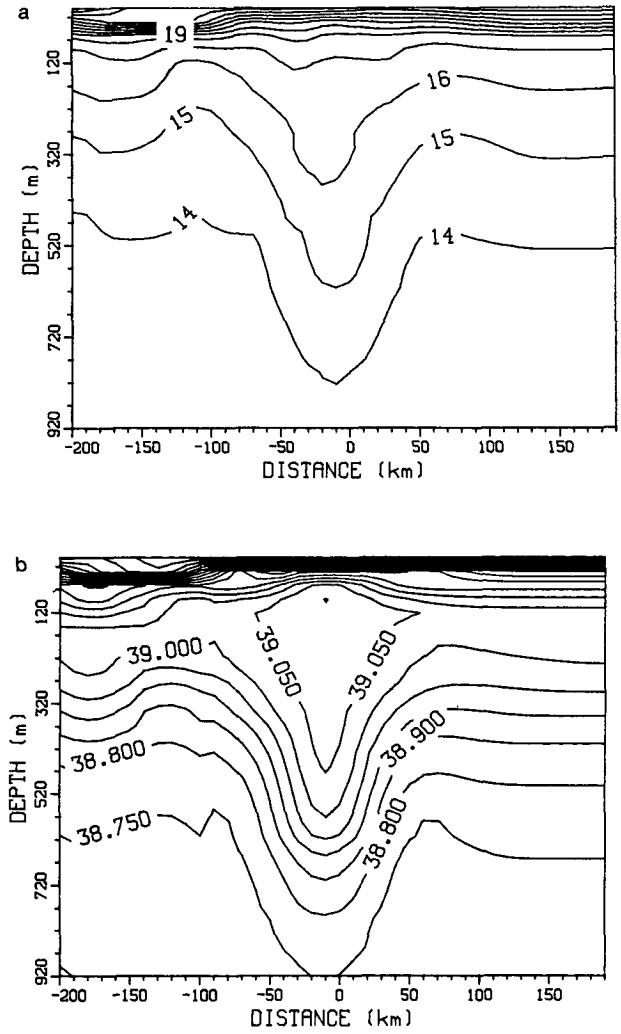

FIG. 9. Vertical cross section through the anticyclonic eddy in October 1984. The eddy center is at 34°N, 34°E. Isolines are (a) temperature (°C) and (b) salinity (parts per thousand). This figure was taken from Feliks and Itzikowitz (1987).

weak 5 cm s^{-1}. This longshore current resembles the Asia Minor current (Ozsoy et al. 1989).

In the vertical velocity, w, inertial oscillations are observed, with large amplitudes in the downwelling zone. During the cyclones the mean (over inertial period) of w is about 0.015 cm s^{-1}. After the cyclone ends the mean w decreases but for another two days the downwelling continues and then stops. The isotherms sink by about 50 m in each cyclone. The mean vertical advection is significant only during the cyclone and two days later when warm and salty water from the upper layers is advected downward.

We examined the influence of basin depth on the evolution by running the model for a case where the bottom depth was 1000 m, all other depths were as in the above experiment. The result show that the downwelling and the alongshore velocity are the same for both experiments.

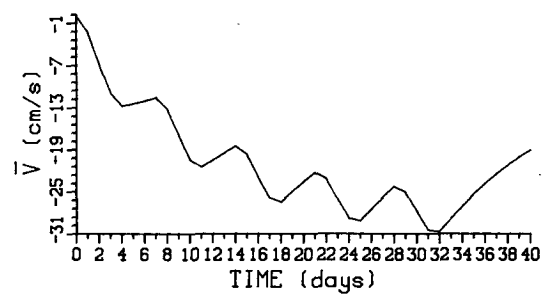

FIG. 10. Time series of $\bar{v}$ between days 0 and 40 at 55 km offshore.

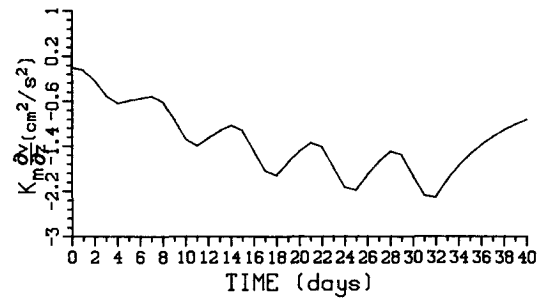

FIG. 11. Time series of the bottom stress $K_m \partial v/\partial z$ between days 0 and 40 at 55 km offshore.

d. *The wind stress*

Description of the Cyprus maritime cyclone is far from complete, and the wind speed is almost unknown

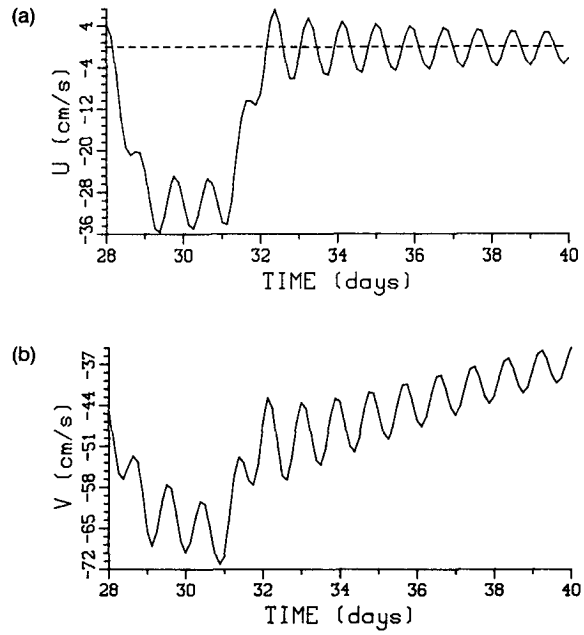

FIG. 12. Time series of (a) u, (b) v, between days 28 and 40 at 55 km offshore at a depth of 11.2 m.

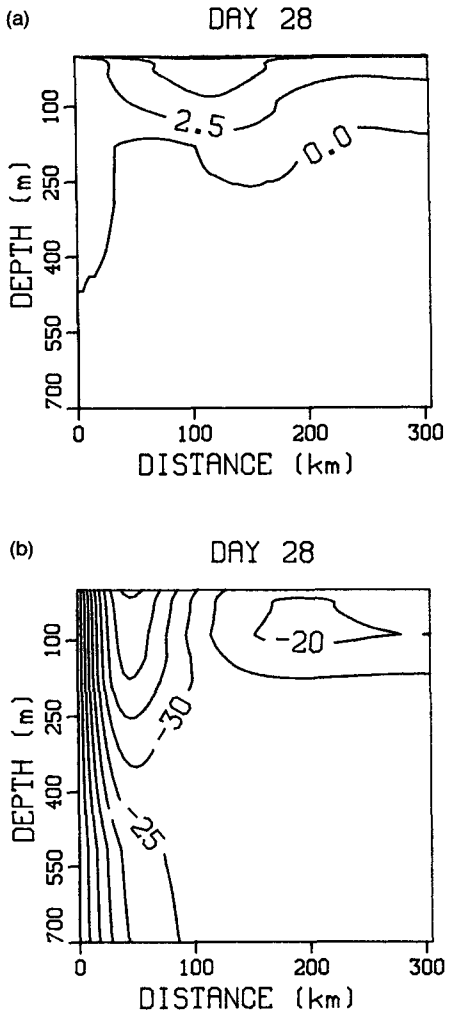

FIG. 13. Vertical cross section of (a) u, (b) v at hour 0 on day 28. Values in cm s^{-1}.

due to lack of observations over the sea. Also there is a large areal variability and differences in intensity of the cyclones. Thus, we study in this section the upper layer evolution in the sea under atmospheric forcing that is weaker than in the first experiment. The wind stress in the following experiments has the same structure as in the first experiment. In the second experiment the maximum stress was 8 dyn cm^{-2} (15 m s^{-1}) and 4 dyn cm^{-2} (10 m s^{-1}) in the third. All other conditions were as in the first experiment.

The evolutions in the sea in these experiments was similar to the evolution in the first. In Figs. 14 and 15 the temperature and alongshore velocity fields are shown for the last two experiments three days after the fourth cyclone ended, and in Figs. 5 and 13 for the first experiment. The main differences between the experiments are

1) a slower downwelling rate obtained as the wind stress decreases. Therefore after the fourth cyclone the isotherms and isohalines sink 70 and 170 m less in experiment 2 and 3 than in the first one.

2) As wind stress decreases, the temperature in the upper 100 m remains warmer, the thermocline is sharper and the depth of the mixed layer is shallower. Therefore, after four cyclones the depth of the mixed layer in the downwelling zone is 250, 200 and 150 m in experiments 1, 2 and 3, respectively.

3) As the wind stress decreases the alongshore jet is weaker and penetrates to shallower depth. Therefore, after four cyclones the jet reaches speeds of 40, 35 and 20 cm s^{-1} in experiments 1, 2 and 3, respectively.

The downwelling front and its associated jet has the same horizontal scale, i.e., maximum speed of the jet is reached 50 km off coast in all three experiments. Thus, we conclude that the horizontal scale of the jet and the downwelling front is independent of strength of the wind stress.

e. The horizontal diffusion coefficient

Only gross estimates of the values of horizontal diffusion coefficients are known. In upwelling problems

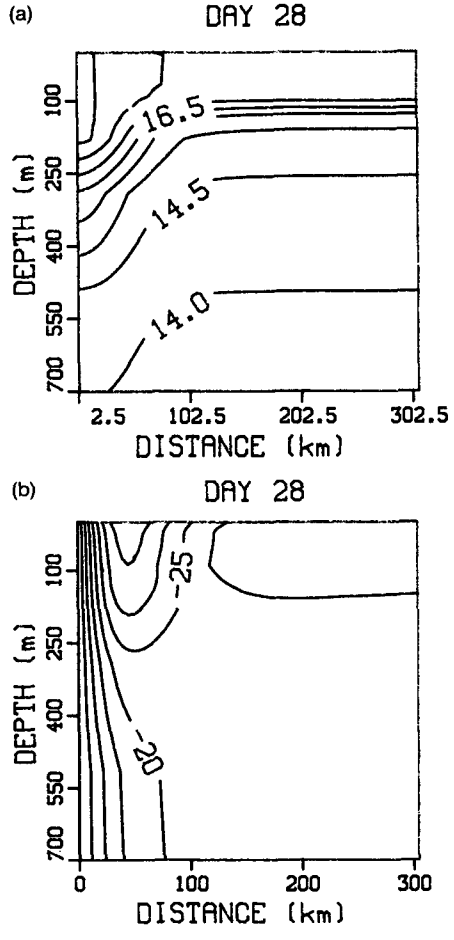

FIG. 14. Vertical cross section of (a) temperature (°C) and (b) alongshore velocity (cm s^{-1}) for experiment 2.

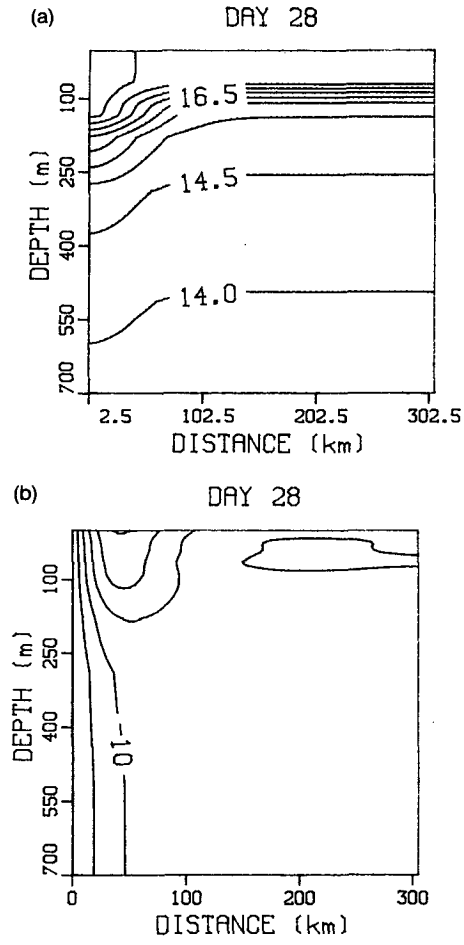

FIG. 15. As in Fig. 14. (experiment 3).

these constants are usually considered to be between 10^6 and 10^9 cm^2 s^{-1} (Shaffer 1974; O'Brien and Hurlburt 1972). The scale of the alongshore current in the upwelling case as given by Allen (1980) is determined by the largest of the following two scales: 1) Rossby radius of deformation and 2) boundary layer scale $\delta x = H_0\sqrt{Kh/Kv}$ where K_h and K_v are the horizontal and vertical diffusion coefficients and H_0 the depth of the sea. Allen's results were obtained for constant N^2, K_h, K_v and H_0. The extent to which boundary layer physics would be operative with vertically variable density stratification (N^2) and eddy coefficient has not been clarified. In our case the Rossby radius of deformation is 11.7 km; since the jet reaches its maximum speed 50 km off coast, it is clear that the boundary layer determines the scale of the jet. Thus, we study in this section the upper layer evolution in the sea under different horizontal diffusion coefficients. In the fourth experiment the horizontal diffusion coefficient for momentum, heat and salinity was 2.5×10^6 cm^2 s^{-1}. The wind stress was as in the third experiment, i.e., the maximum stress was 4 dyn cm^{-2}. We compare the results of this experiment with those of the third experiment. In Figs. 15 and 16 the temperature and alongshore velocity fields of the third and fourth experiments are shown for 3 days after the fourth storm. Significant differences were obtained. The downwelling and the jet horizontal scale is much smaller in experiment 4. The jet reaches its maximum speed 30 km off the coast in experiment 4 and 50 km in experiment 3. The vertical scale is much larger in the fourth experiment and so the jet speed. Let L_3 and L_4 denote the horizontal scale of the jet in experiments 3 and 4 and be equal to the distance between location of the maximum speed of the jet and the coast. It is found that the ratio $L_4/L_3 = 0.6$. The ratio of the square root of the (sum of the) horizontal diffusion coefficients for heat and momentum in experiments 4 and 3 is

$$[(2.5\ 10^6 + 2.5\ 10^6)/(5\ 10^6 + 10\ 10^6)]^{1/2} = 0.58$$

i.e., the scale of the jet is almost proportional to the square root of the horizontal diffusion coefficient.

f. The vertical exchange coefficient

In the formulation of the vertical exchange coefficient we adopt the concept of mixing length, l, (3.16).

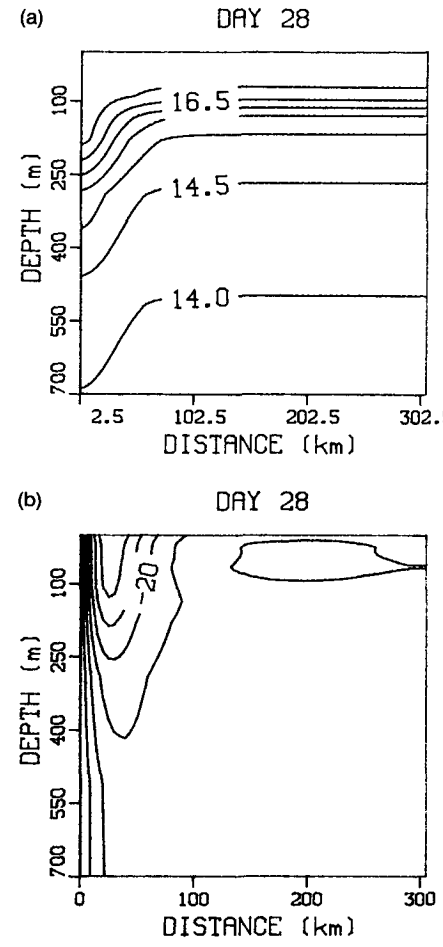

FIG. 16. As in Fig. 14. (experiment 4).

In that formulation Z_m is the depth where the maximal value of l is attained. The roughness parameter z_0 is smaller by two orders of magnitude with respect to the smallest vertical grid integral; thus its influence on the value of l and consequently on the vertical exchange coefficient is negligible.

In this section we study the evolution under different values of Z_m. The next experiment is similar to the first experiment except Z_m = 15 m, while in the first Z_m = 35 m. In Fig. 17 the temperature and alongshore velocity fields are shown after four storms. In Fig. 18 the vertical profiles of temperature and vertical exchange coefficient at different times are shown. The downwelling is very similar to the first experiment. The most prominent differences are that in the open sea the mixed layer depth is 65 m whereas in the first experiment it is 100 m. Temperature in the mixed layer is warmer by 0.5°C, and the thermocline is significantly sharper, i.e., the summer thermocline persists for a longer time in the last experiment. These differences are the result of weaker vertical mixing. The weaker mixing is the result of a smaller velocity exchange coefficient, which is three times smaller than in the first

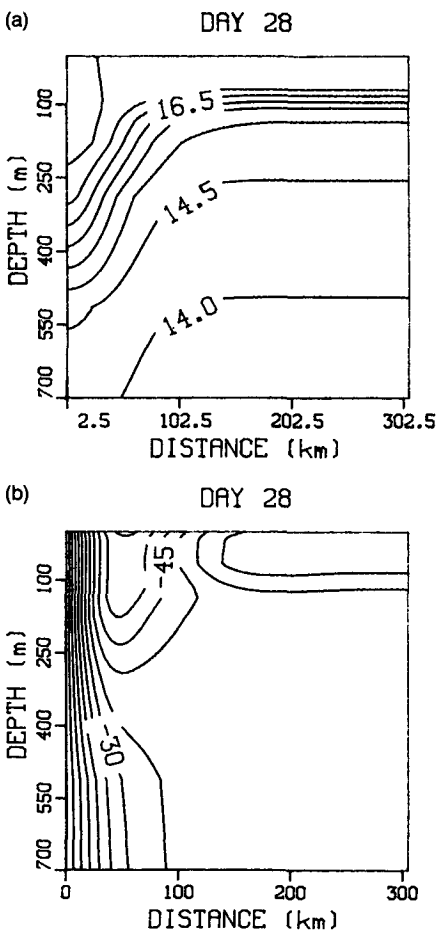

FIG. 17. As in Fig. 14 but for experiment 3.

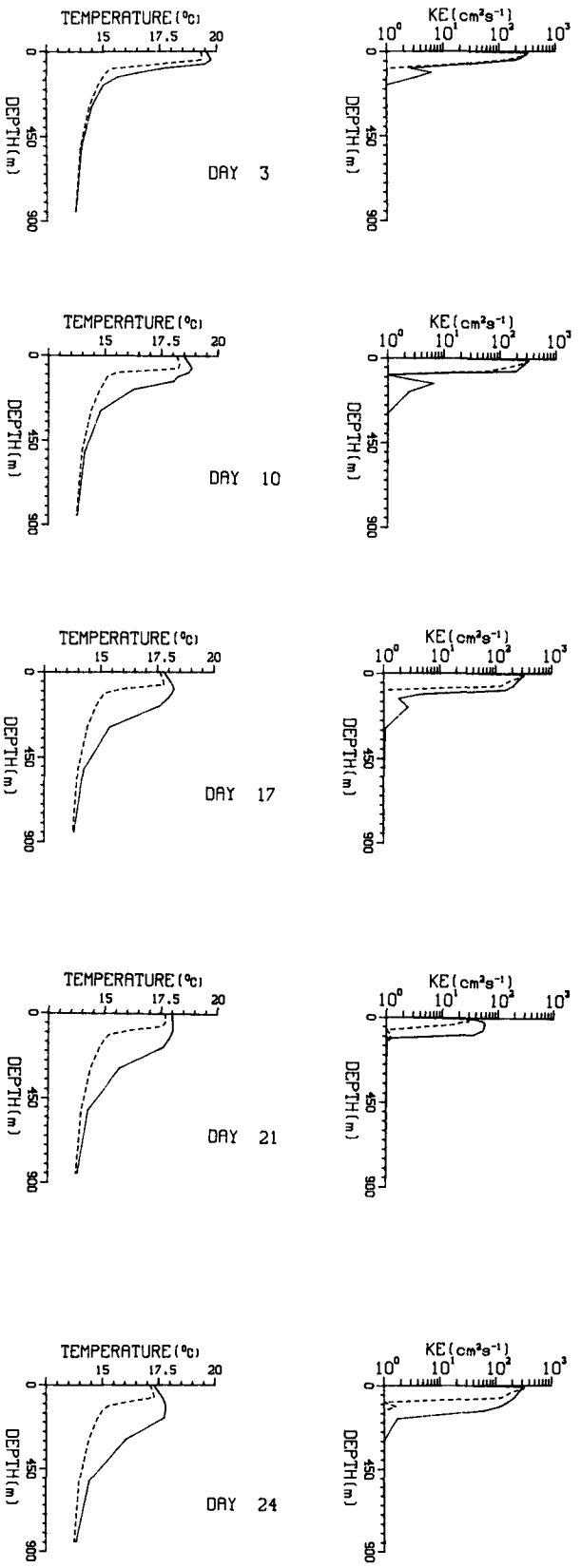

FIG. 18. As in Fig. 6 but for experiment 4.

experiment during the storms (Figs. 6 and 18). Below the mixed layer vertical temperature profiles are almost the same in both experiments—even in the downwelling zone. That is, the evolution in the mixing layer does not influence downwelling below the mixing layer. During calm periods between the storms the vertical exchange coefficient decreases by an order of magnitude in both experiments. However, in the first experiment the decrease is faster due to faster adjustment of the vertical stratification.

The jet along the coast is stronger in the last experiment (Figs. 13 and 17). This is due to the larger isotherm slope in the downwelling front (Figs. 5 and 17). The horizontal scale of the jet in both experiments is the same even though the vertical exchange coefficient in the mixed layer during the storms is three times larger in the first experiment.

g. The initial stratification

In the above experiments the initial stratification was measured 100 km south of Turkey in October 1983 (Fig. 3). In this section we study the evolution from an initial stratification, taken from the average autumn profiles of the eastern Levantine Basin; these profiles are shown in Fig. 19. The main differences between the two stratifications are 1) the main thermocline is sharper in the average profiles and 2) the salinity reaches its maximum at a depth of 250 and 100 m in the average and Turkey profiles, respectively. The Rossby radius of deformation is 14.4 km in the average profiles compared to 11.7 km in the former case. In the next experiment the average profiles were taken as the initial stratification, all others were as in the first experiment.

In Fig. 20 the temperature and alongshore velocity fields are shown 3 days after the fourth storm for the average initial condition experiment (compare to Fig. 4 of the first experiment). The main differences between the two experiments are 1) The 14.5°–16.5°C isotherms downwelled 160 m in the last experiment, while in the first the 16.5°C isotherm lowered by 140 m and that of 14.5°C by 200 m. This difference is due to the difference in stability of the initial profile. In the first experiment the isotherms around 16.5°C were located in a more stable environment and sank less, while the isotherms around 14.5°C resided in a less stable environment and sank more than in the last experiment. The temperature in the mixed layer was warmer by 1°C in the last experiment. This result is due to the intensive mixing in the upper 100 m in both cases; in the last experiment the initial profile is significantly warmer in the upper 100 m (except in the 20 m near the sea surface) than in the first. The alongshore jet was stronger by 10 cm s^{-1} and penetrated downward 100 m farther.

The horizontal scale of the coastal jet and the downwelling is the same as in the first experiment. Since the Rossby radius of deformation is much smaller than the jet scale, the horizontal boundary layer determines the scale of the jet.

5. Summary

The most prominent winter storms in the eastern part of the eastern Levantine Basin are the Cyprus cyclones. The center of the cyclones is located between Cyprus and 200 km to the west. Surface wind speeds reach 15–30 m s^{-1}, and the air temperature is about 10°C or less. The radius of the cyclones is between 500 and 1500 km. Such cyclones can persist for 2–4 days, and about five of them are observed in a typical year.

A numerical simulation of the evolution in the sea under an atmospheric forcing that resembles five successive Cyprus cyclones, was carried out with a two-dimensional numerical model. Initial temperature and salinity profiles were taken from observation at the end of summer south of Turkey. The numerical results show that two distinct regions are obtained: a downwelling zone near the coast (about 100 km wide), and the open sea, where almost horizontal homogeneity exists.

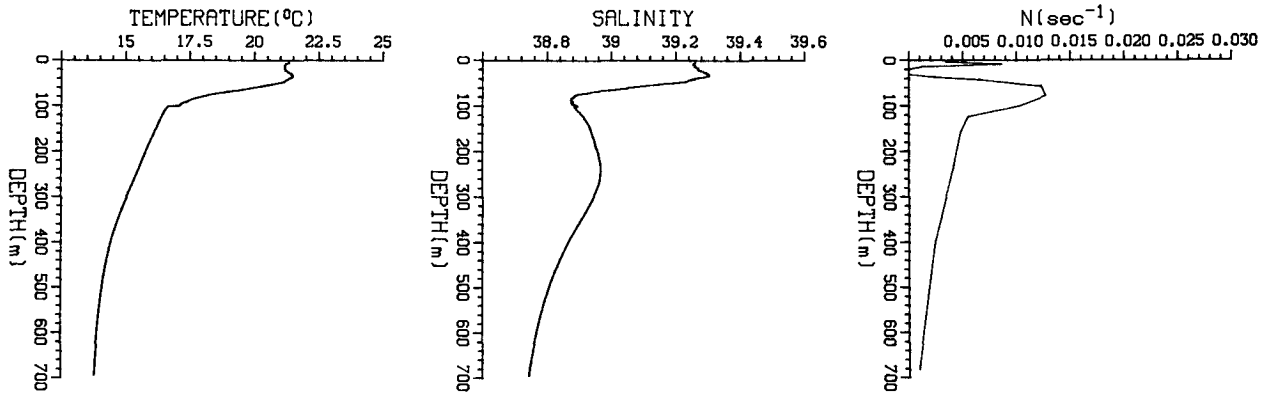

FIG. 19. As in Fig. 3 but for the average profiles.

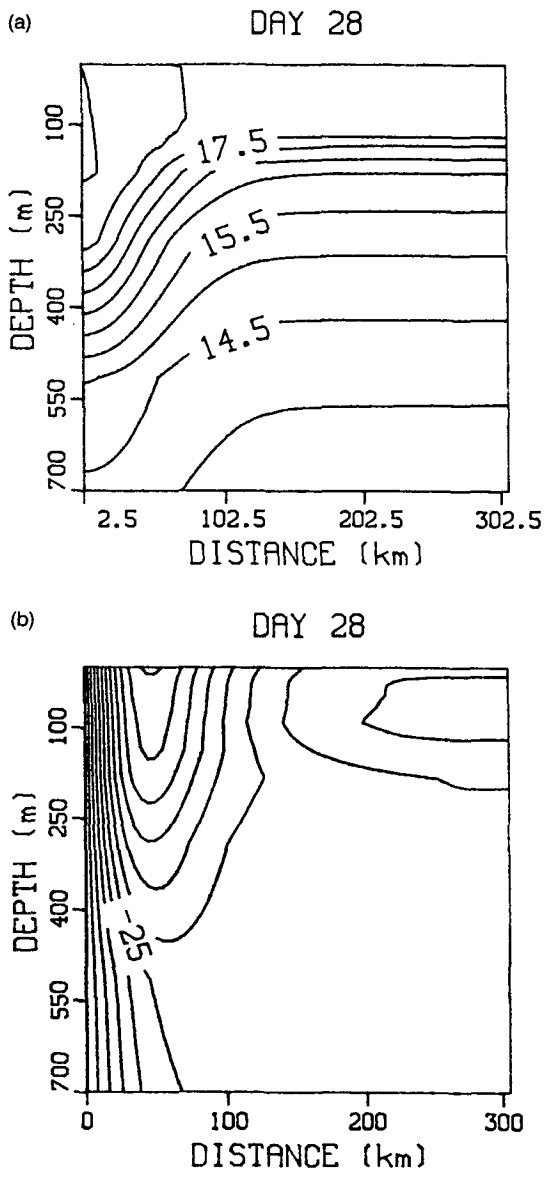

FIG. 20. As in Fig. 14 but for average profiles.

In the open sea zone after the fifth cyclone, the mixed layer depth was about 150 m, its temperature was 16°C and its salinity 39.05. This water type characterizes the LIW in its formation region. We suggest that the LIW is formed in the region influenced by the Cyprus cyclones.

Intensive downwelling is observed in a band of 100 km adjacent to the coast. The 14°–17°C isotherms downwelled by more than 250 m. In this zone a very deep mixed layer, more than 300 m thick, is obtained. The warm water is observed also at the sea surface in a band 50 km wide. In wintertime IR images a similar band of warm water is observed along the coast of Asia Minor and the northeast coast of the Mediterranean. We assume that this band is a surface manifestation of the downwelling zone.

In the horizontal and vertical current, inertial oscillations are obtained during stormy and calm periods. The oscillations form in the upper layer and propagate downward; oscillations in temperature and salinity are small. The mean (over inertial period) of the cross-shore component of the velocity in the upper level during the storm is about 30 cm s^{-1} directed toward the coast, but during the calm weather it is very small. So advection is important only during the storms. This advection advects cool water from the open sea toward the downwelling zone, and causes an inversion in the upper levels. This inversion disappears due to intensive vertical mixing several days after the storm ends.

In the longshore component of the velocity, a coastal jet is obtained in the downwelling zone. The mean jet velocity over an inertial period is in geostrophic balance with the mean pressure gradient. It attains a maximum speed about 50 km off coast near the sea surface. This jet resembles the Asia Minor current, which suggests that this current develops in a similar way during the winter storms.

Temperature and salinity profiles in the downwelling zone are very similar to those observed in the warm and salty core eddies in the Levantine Basin; particularly along the coast of Asia Minor, Feliks and Itzikowitz (1987), Ozsoy et al. (1989). We assume that those eddies form along the coast of Asia Minor. Meandering in the temperature front during winter is observed in IR satellite images along the Asia Minor coast, and the series of anticyclonic eddies, which masked the Asia Minor current observed by Ozsoy et al. (1989), support this assumption. Baroclinic instability mechanisms were suggested for the upwelling zone of the California Current system by Mysak (1977), Hukuda (1982) and Ikeda (1983) to explain the meandering of the upwelling front and development of eddies found there. Due to the similarity between the front and the jet in the downwelling and upwelling regions, we suggest that similar mechanisms may act here also.

Study of some parameters and the effect of the initial conditions and atmospheric forcing show that the downwelling and alongshore jet does not change if we change the sea depth between 1000 and 2000 m. The horizontal scale of the downwelling and the coastal jet is proportional to the square root of the horizontal diffusion coefficient. This horizontal scale is not a function of the intensity of wind stress, the initial stratification (in case where the Rossby radius of deformation is small), nor the values of the vertical exchange coefficient during the storms. The rate of downwelling increases with increasing wind stress, decreasing horizontal diffusion coefficient, and decreasing stability. The evolution in the mixing layer does not influence the downwelling rate below the mixing layer. The coastal jet speed increases as the mixing decreases.

The effects of the complexity of the weather system, the influence of topography, the curvature of the coastline and the curl of wind stress on the evolution in the downwelling zone need to be examined.

Acknowledgments. I am happy to thank Dr. D. Anati and Dr. E. Gavze for discussion, helpful suggestion and careful reading of this paper. Senior Forecaster Mr. Y. Barkan drew the surface synoptic maps. This research was partially supported by ONR Grant N0014-89-J-1845.

REFERENCES

Allen, J. S., 1980: Models of wind-driven currents on the continental shelf. *Ann. Rev. Fluid Mech.*, **12,** 389–433.

Alpert P., B. U. Neeman and Y. Shay-El, 1990: Climatological analysis of Mediterranean cyclones using ECMWF data. *Tellus,* **42A,** 65–77.

Brenner, S., 1989: Warm core eddies in the Eastern Mediterranean. *J. Geophys. Res.*, **94,** 12 593–12 602.

Csanady, G. T., 1984: *Circulation in the Coastal Ocean.* D. Rediel, 279 p.

Feliks, Y., 1990: Isolated vortex evolution in a 2 and a 4 mode models. *Deep-Sea Res.*, **137,** 571–591.

——, and S. Itzikowitz, 1987: Movement and geographical distribution of anticyclonic eddies in the Eastern Levantine Basin. *Deep-Sea Res.*, **34,** 1499–1508.

Fofonoff, N. P., and R. C. Millard Jr., 1983: Algorithms for computation of fundamental properties of seawater. UNESCO Tech. Pap. in Mar. Sci. No 44, 53 pp.

Gonella, J., 1971: A local study of inertial oscillations in the upper layers of the ocean. *Deep-Sea Res.*, **18,** 775–788.

Haltiner, G. J., and T. Williams, 1980: *Numerical Prediction and Dynamic Meteorology,* 2nd ed. J. Wiley, 477 p.

Hecht, A., N. Pinardi and A. R. Robinson, 1988: Currents, water masses, eddies and jets in the Mediterranean Levantine Basin. *J. Phys. Oceanogr.*, **18,** 1320–1353.

Hukuda, H., 1982: Subharmonic destabilization off Vancouver Island. *J. Phys. Oceanogr.*, **12,** 285–292.

Huss, A., and Y. Feliks, 1981: A mesometeorological numerical model of the sea and land breezes involving sea–atmospheric interactions. *Beitr. Phys. Atmos.*, **54,** 238–257.

Ikeda, M., 1983: Linear instability of a current flowing along a bottom slope using a three-layer model. *J. Phys. Oceanogr.*, **13,** 208–223.

Madala, R. V., and S. A. Piacsek, 1977: A semi-implicit numerical model for baroclinic oceans. *J. Comput. Phys.*, **23,** 167–178.

Marchuk, G. I., 1975: *Methods of Numerical Mathematics.* Springer, 316 pp.

Mysak, L. A., 1977: On the stability of the California undercurrent off Vancouver Island. *J. Phys. Oceanogr.*, **7,** 904–917.

O'Brien, J. J., and H. E. Hurlburt, 1972: A numerical model of coastal upwelling. *J. Phys. Oceanogr.*, **2,** 14–26.

Ozsoy, E., A. Hecht and U. Unluota, 1989: Circulation and hydrography of the Levantine Basin: Results of POEM coordinated experiments 1985–1986. *Progress in Oceanography,* Vol. 22, Pergamon, 125–170.

Ozturgut, E., 1976: The source and spreading of Levantine Intermediate Water in the Eastern Mediterranean. Saclant ASW Res. Center Memo. SW-92, La-Spezia, Italy, 45 pp.

Pandolfo, J. P., and C. A. Jacobs, 1973: Tests on urban meteorological pollutant model using co-validation data in Los-Angeles metropolitan area. Center for Environment of Man, 172 p. [CEM Rep. 490a].

Shaffer G., 1974: On the North West African coastal upwelling system. Ph.D. thesis, Institut fur Meereskunde, Universtat Kiel.

Sverdrup, H. U., M. W. Johnson and R. H. Fleming, 1954: *The Oceans,* Prentice–Hall, 1087 p.

Thompson, R., 1974: Predicting the characteristic of the well-mixed layer. WHOI Tech. Rep. WHOI-74-82.

Unluata, U., T. Oguz and E. Ozsoy, 1983: Blocking of steady circulation by coastal geometry. *J. Phys. Oceanogr.*, **13,** 1055–1062.

Wust, G., 1961: On the vertical circulation of the Mediterranean sea. *J. Geophys. Res.*, **66,** 3261–3271.